Nanoscale

PAPER

View Article Online
View Journal | View Issue

Cite this: *Nanoscale*, 2020, **12**, 6438

Highly conductive and transparent coatings from flow-aligned silver nanowires with large electrical and optical anisotropy†

Ye Xu, *‡[a,b,c] Dengteng Ge, ‡[d,e] Gabriel A. Calderon-Ortiz,[b,f] Annemarie L. Exarhos, §[b] Coline Bretz,[c] Ahmed Alsayed,[c] Dave Kurz,[b] J. M. Kikkawa,[b] Remi Dreyfus,[c] Shu Yang [d] and A. G. Yodh[b]

Received 11th November 2019,
Accepted 13th February 2020

DOI: 10.1039/c9nr09598e

rsc.li/nanoscale

Conductive and transparent coatings consisting of silver nanowires (AgNWs) are promising candidates for emerging flexible electronics applications. Coatings of aligned AgNWs offer unusual electronic and optical anisotropies, with potential for use in micro-circuits, antennas, and polarization sensors. Here we explore a microfluidics setup and flow-induced alignment mechanisms to create centimeter-scale highly conductive coatings of aligned AgNWs with order parameters reaching 0.84, leading to large electrical and optical anisotropies. By varying flow rates, we establish the relationship between the shear rate and the alignment and investigate possible alignment mechanisms. The angle-dependent sheet resistance of the aligned AgNW networks exhibits an electronic transport anisotropy of ~10× while maintaining low resistivity (<50 Ω sq^{-1}) in all directions. When illuminated, the aligned AgNW coatings exhibit angle- and polarization-dependent colors, and the polarized reflection anisotropy can be as large as 25. This large optical anisotropy is due to a combination of alignment, polarization response, and angle-dependent scattering of the aligned AgNWs.

Introduction

The large aspect ratio and electrical conductivity of silver nanowires (AgNWs) offer promising ingredients for emerging electronic and optical applications, including conducting inks and pastes used in circuits.[1,2] AgNW films, for example, are attractive candidates for transparent conductive coatings in flexible touch-screen displays, due to their high visible light transparency and tolerance to planar strain.[3–5] Moreover, the one-dimensional (1D) nature of these wires induces anisotropy in electrical conductivity and optical appearance, and some nanowire assemblies with anisotropic properties have been found to exhibit enhanced performance in nanocomputing devices,[6] antennas,[7–9] polarized-light-based sensors,[10] and surface enhanced Raman spectroscopy (SERS).[11]

The performance of AgNW-based devices usually depends on the density and organization of the AgNWs. When AgNWs are used in flexible electronics to replace ITO, the combination of a *low areal* density for optical transparency and a percolated network of AgNWs for conductivity is required. In the literature, this performance is generally achieved from *isotropic* percolating nanowire networks at a *low areal* density.[5,12–14]

Films with a *high areal* density of AgNWs, on the other hand, offer the possibility to generate *anisotropic* optical and electrical properties that ultimately offer many more ways to modulate signals. For example, the fabrication of AgNW-based optical elements with polarization sensitivity and the synthesis of conducting devices with anisotropic conductivity require both a high degree of alignment and a large areal density. In a related vein, the creation of plasmonic waveguides, based on single[15–17] or multiple[9,18] nanowires, could rely on plasmonic interactions among nanowires,[19] which would benefit from aligned nanowires with high areal density. To this end, films

[a]*School of Mechanical Engineering and Automation and Center of Soft Matter Physics and its Applications, Beihang University, Beijing 100191, P.R. China. E-mail: ye.xu@buaa.edu.cn*
[b]*Department of Physics and Astronomy, University of Pennsylvania, Philadelphia, Pennsylvania 19104, USA*
[c]*Complex Assemblies of Soft Matter, CNRS-Solvay-UPenn UMI 3254, Bristol, Pennsylvania 19007, USA*
[d]*Department of Materials Science and Engineering, University of Pennsylvania, Philadelphia, Pennsylvania 19104, USA*
[e]*State Key Laboratory for Modification of Chemical Fibers and Polymer Materials, Institute of Functional Materials, Donghua University, Shanghai 201620, P.R. China*
[f]*Department of Physics and Electronics, University of Puerto Rico at Humacao, Humacao, Puerto Rico 00791, USA*
†Electronic supplementary information (ESI) available. See DOI: 10.1039/c9nr09598e
‡Authors of equal contributions.
§Present address: Department of Physics, Lafayette College, Easton, PA 18042, USA.

Table 1 Comparison of electrical and optical properties of AgNW films prepared with different alignment methods

Sample preparation	Alignment quantified?	Areal density/ fraction	Sheet resistance	Electrical anisotropy	Transparency	Linear optical anisotropy	Patterning?	Scale
Self-assembly at the water–oil interface[25]	N	Close-packed	NM	NM	NQ	NQ	N	10 mm
Langmuir–Blodgett[30]	N	Close-packed	NM	NM	NQ[a]	NQ	N	50 mm
Flow through a circular capillary tube[11]	N	NQ[b]	NM	NM	NQ	~2	N	300 μm[c]
Capillary printing[31]	Y	0.3–20%	10–50 Ω sq^{-1}	~1.7	90–95%	NM	N	10 mm
Meniscus-dragging[32]	N	3–12 × 10^4 NW mm^{-2}	10 Ω sq^{-1}	NM	70–95%	1.5	N	10 mm
Dip-coating[42]	Y	0.3–2.6%	50–10^7 Ω sq^{-1}	1.06–27.6	97–99%	NM	N	25 mm
H-dip[33]	N	NQ	2–7 Ω sq^{-1}	1.2	60–80%	2–3	N	100 mm
Bar-coating[34]	Y	NQ[b]	NA	NA	80–95%	~4	N	200 mm
Microfluidics (this work)	Y	10^4 NW mm^{-2}	3–5 Ω sq^{-1}	~10	70–80%	~25	Y	~5 mm wide

Y: yes; N: no; NM: not measured; NQ: not quantified. [a] Transmission spectra were measured but the intensities were not quantified. [b] Micrographs of nanowire coatings are shown but the areal densities were not quantified. [c] Diameter of the inner surface of the capillary tube.

of aligned nanowires offer the possibility to tune the coupling between individual nanowires and thus introduce novel collective responses, which could be more sensitive than conventional, continuous metal films. Moreover, nanowire films have potential to be flexible and stretchable, which could also be useful for mechano- and thermal-sensing.

Many methodologies for deposition and alignment of 1D nanomaterials such as nanowires or nanotubes have been explored.[10,11,20–29] Self-assembly at oil–water–air interfaces[25] and the Langmuir–Blodgett method[30] have been used to align AgNWs. More recently, capillary-based techniques including capillary printing,[31] meniscus-dragging,[32] H-dip,[33] and bar-coating[34] have been used to create large-scale aligned or cross-aligned AgNW coatings on flat substrates. Nevertheless, these techniques can only print AgNWs along one specific direction,[32,33] or require an external mechanical force.[31] Therefore, they are not suitable for parallel printing of complex circuitry. In microfluidic channels, the shear force and flow geometry can be well-controlled, thus offering more flexibility for depositing AgNW coatings with pre-designed patterns. Indeed, shear flow has been used for aligning nanotubes and nanowires. Huang *et al.* first explored this method to align nanowires within microfluidic apparatus.[35] They created nanoscale network structures with a very low areal density. Later, Liu *et al.* employed shear flow in circular glass capillaries to prepare more dense and aligned AgNW coatings.[11] Though very efficient, because of geometric constraints, these nanowires cover only the interior of circular glass tubes. Clearly, there remains a need for new methods to assemble AgNWs into scalable and aligned structures of high areal density with adequate light transmission, to achieve electrical and optical anisotropy for applications such as polarization light sensors and plasmonic waveguides.

In this contribution, we employed flow-assisted assembly to generate centimeter-scale AgNW coatings at high areal density (approximately 40% areal coverage or 10^4 nanowires per mm^2), with high conductivity (<10 Ω sq^{-1}), and with controlled electrical and optical anisotropy on planar surfaces. This robust method enables experimental control of alignment *via* variation of the shear rate of the AgNW suspension near the substrate surface. We systematically investigated the angular dependence of coating sheet resistance and optical properties. These properties are strongly affected by AgNW alignment. The anisotropy of electrical conductivity is approximately 10× in well-aligned AgNW coatings. Moreover, by combining polarized illumination and detection of scattered light from the aligned AgNW coatings, the degree of polarized reflection anisotropy can reach up to 25×. The coatings also have good transparency (~70%) in normal incidence across the visible spectrum. The performance and features of AgNW coatings based on our deposition technique, along with those from previous literature, are reported in Table 1. Our transparent coatings in the planar geometry have a comparatively high areal density and larger electrical and optical anisotropy due to better control of AgNW orientation and concentration. These features make them attractive for use as components in micro-/nano-circuits and optical sensors.

Results and discussion

Preparation of AgNW coatings

Thin coatings of AgNWs are prepared by flowing nanowire suspensions through thin rectangular microfluidic channels, as shown in Fig. 1A. At the beginning of the coating preparation, we utilize a syringe pump (Harvard Instrument) to drive a flow of 2 mL of nanowire suspension through the channel at a constant volumetric flow rate, Q, ranging from 0.5 to 5 mL min^{-1}. The flow of the AgNW suspension creates boundary shear at a rate ranging from 10 s^{-1} to 1000 s^{-1} near the top

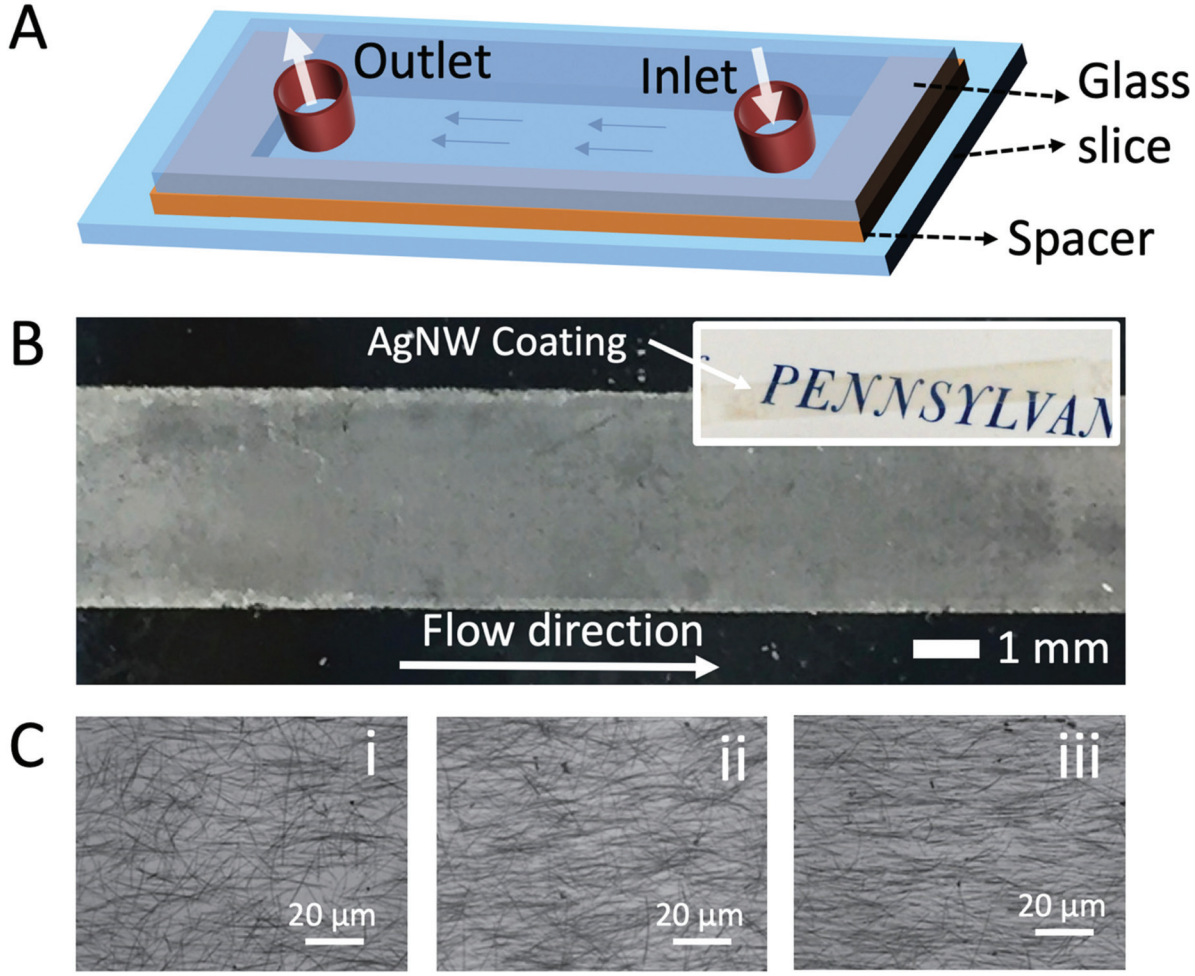

Fig. 1 (A) Schematic of flow channels for preparing silver nanowire coatings. (B) Low magnification optical image of the deposited AgNW coating of approximately 40% areal coverage, showing centimeter-scale uniformity. Inset: photograph of the same AgNW coating taken on top of the text, showing its transparency. (C) High magnification optical images of AgNWs deposited under different flow conditions. The shear rates of the AgNW suspension near the glass substrate are 15 s^{-1} (i), 100 s^{-1} (ii), and 500 s^{-1} (iii), respectively.

and bottom glass walls of the channel, respectively. As a result, a fraction of the nanowires are observed to deposit onto the glass slide surface that is exposed to the AgNW suspension. Subsequently, 1 mL pure ethanol is flowed through the channel to remove excess nanowire suspension, followed by a gas purge and drying to remove liquid remaining inside the channel. AgNWs deposited on the top and bottom walls of the channel are not washed out with the main flow because the van der Waals forces are of order 10^{-6} N (ref. 36) between the nanowire and the glass slide and are therefore strong enough to prevent the shear flow forces (of order 10^{-9} N) from displacing the nanowire. At the end of the preparation process, a uniform thin layer of AgNWs forms at the surface of each glass slide as shown in Fig. 1B. The coated glass slides are then separated for further characterization.

As shown in Fig. 1C–E micrographs, nanowires coated on the surface of the glass slides exhibit increased alignment with increasing suspension flow rate through the channel. The deposited nanowires are poorly aligned at low flow rates, *i.e.* 0.5 mL min^{-1}, as shown in Fig. 1C-i. With increasing flow rate, *i.e.* to 2 mL min^{-1} and 5 mL min^{-1}, the deposited nanowires begin to align along the flow direction over the whole area inside the microchannels (Fig. 1C-ii and iii). While the aspects of this flow alignment effect have been explored and utilized in previous studies,[11,20,35,37,38] the present experimental methods provide a simple and robust way to generate centimeter-scale and potentially patternable AgNW coatings on a flat substrate with high areal density and controlled alignment.

Alignment of AgNWs

We characterize the microscopic structure of nanowire networks by analyzing the micrographs obtained by both optical and scanning electron microscopy (SEM). Examples of micrographs are shown in Fig. 2A–C. They are taken from samples prepared at three different suspension flow rates: 0.5, 2, and 5 mL min^{-1}, respectively. For analysis, each individual nano-

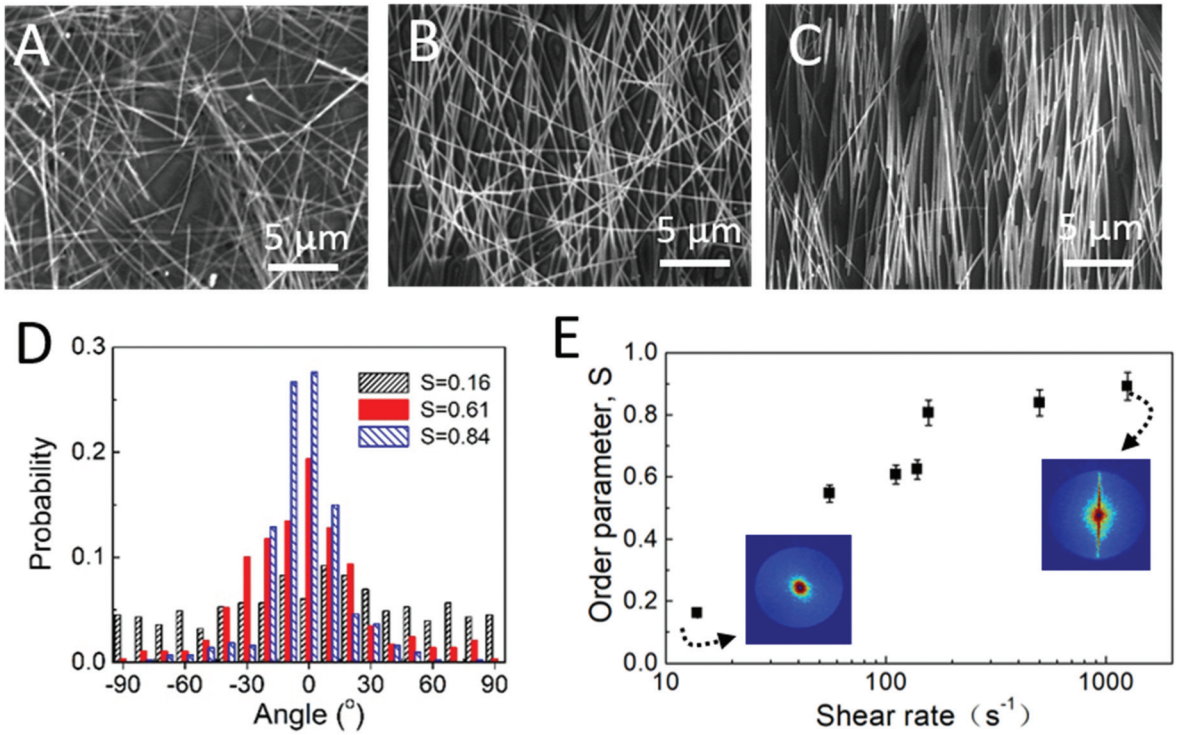

Fig. 2 (A–C) SEM images of three AgNW coatings to illustrate analysis of the orientations of individual nanowires. (D) Histogram of the angle between the nanowire orientation and flow direction for three representative samples seen in Fig. 1C with different order parameters: S = 0.16 (A), =0.61 (B), and 0.84 (C). (E) Order parameter of deposited AgNW coatings, S, as a function of shear rate of the flowing AgNW suspensions near the glass substrate, γ. Insets: light scattering patterns of a random and well-aligned AgNW coating in k-space. The colors show the intensity of the scattered laser light with red as the highest intensity and blue as the lowest intensity.

wire in the field of view is approximated by a straight-line segment. The orientation, θ, and length, l, of the AgNW are then recorded by image processing using the software ImageJ. Here we define $\theta = 0°$ as the direction of the flow.

The distributions of the nanowire orientation are shown in the histograms in Fig. 2D. For the image in Fig. 2A, the probability distribution is very broad and flat, suggesting a predominately random distribution of the nanowire orientation. By contrast, the probability distribution of nanowire orientation from images in Fig. 2B and C exhibits a clear peak near $\theta = 0°$. The presence of these peaks clearly demonstrates that the orientations of deposited AgNWs are biased toward the flow direction. These different distributions of nanowire orientation are also consistent with the intensity patterns generated by laser light scattering. As shown in the insets of Fig. 2E, the AgNW coating with a random distribution of nanowire orientation exhibits a nearly isotropic scattering pattern in the k-space, while the one with aligned AgNWs exhibits a strongly anisotropic scattering pattern.

We further quantify alignment by the two-dimensional nematic order parameter defined as[39,40]

$$S = 2\langle \cos^2 \theta \rangle - 1. \quad (1)$$

where $S = 0$ corresponds to a random distribution and $S = 1$ corresponds to perfect alignment. Using the distribution of θ in Fig. 2D, the three samples shown in Fig. 2A–C give S values of 0.16, 0.61, and 0.84, respectively.

The shear rate near the glass surfaces plays an important role in controlling the degree of alignment of AgNWs in these flow-deposited coatings. Given the density, ρ, viscosity, μ, and flow rate, u, of the AgNW suspension, together with the geometry of the channel (height, H, and width, W), the Reynolds number, $\mathrm{Re} = \rho u H/\eta$, is of order 10^{-2}. This indicates that flow is laminar. Therefore, assuming no-slip boundary conditions, for a volumetric flow rate, Q, the shear rate near the wall can be calculated as $\gamma = 6Q/(H^2W)$. In Fig. 2E, we plot the nematic alignment order parameter of the deposited AgNW coatings *versus* shear rates. The suspended nanowires that have made point-contact with the glass surface respond to the high shear rate near the surface, introduced by the rapid channel flow, by adopting a preferred orientation parallel to the flow.

To better understand the flow-induced alignment behaviors, we perform semi-quantitative analyses on experimental observations. We first rule out gravity or sedimentation effects, since AgNWs adhere equally to both top and bottom surfaces of the thin channel. Therefore, a possible explanation for the effect of flow-induced alignment could derive from a competition between directional shear flow and random rotational diffusion of the AgNWs. At a low shear rate, the rotational diffusion dominates and gives rise to a more isotropic organiz-

ation of the AgNWs, but at large shear rates the flow defines the orientation. We then estimate the Peclet number (Pe) for the AgNW suspension, defined by the ratio between the shear rate and the rotational diffusion constant of the nanowire, D_r, as[33,41] $\mathrm{Pe} = \dot{\gamma}/D_r = \pi\dot{\gamma}\mu L^3/4k_BT$, where $\mu \approx 1.2$ mPa s is the viscosity of the AgNW suspension and $L \approx 30$ μm is the average length of AgNWs. For the range of experimental shear rates, $\dot{\gamma} = 10$ to $1000\ s^{-1}$, Pe is of the order of 10^6 to 10^8. The large Pe implies that shear flow should dominate over rotational diffusion in all the experimental flow conditions used for preparing AgNW coatings. We believe that the key to the alignment of nanowires on the glass surface occurs when the rods make contact with the surface (*i.e.* rather than in the bulk fluid). Just after making contact, and assuming that this contact occurs at one end of the nanowire with the other end free, the nanowires can pivot and will respond to flow shear-stresses near the surface. Here, the most plausible mechanism is a competition between electrostatic forces that pull the nanowire to the glass substrate and the hydrodynamic drag force of the shear flow that rotates the AgNWs along a direction parallel to the flow when they get contact with the glass surface. Here, by assuming a line charge density δ for the nanowire and a surface charge density σ for the glass surface, we can estimate the ratio between electrostatic torque (M_{elec}) and hydrodynamic torque (M_{hydro}),

$$\frac{M_{hydro}}{M_{elec}} \sim \frac{4}{3}\frac{\gamma\eta L\varepsilon_0\varepsilon_r}{\delta\sigma} \quad (2)$$

where $\varepsilon_0\varepsilon_r$ is the electrical permittivity of the AgNW suspension. The detailed illustration of those two torques can be found in the ESI.† With increasing shear rate, γ, it is possible to transition from an electrostatic-dominated regime to a shear-flow-dominated regime. In the former regime, AgNWs are pulled down to the glass surface with random orientations before they can be aligned by flow; in the latter region, AgNWs are quickly aligned by the high shear rate near the surface. In our experiments, given the glass surface charge on the order of 1 mC m^{-2}, and a transition of shear rate at approximately γ = 100 s^{-1}, according to eqn (2), the nanowires carry a line charge density on the order of 3×10^{-12} C m^{-1}, or 20 effective charges per micron. Although further experimental confirmation of these predictions is difficult, the estimation is plausible for the observed transition of the AgNW orientation as a function of the shear rate near the surface.

Electrical conductivity and anisotropy

One advantage of our system *versus* the literature[11] is that we can break apart the microchannel to characterize the electrical resistance of the AgNW coatings on the surface of glass slides. To explore the angle-dependence of surface conductivity in our AgNWs coatings, we use a four-point probe setup and a rotating stage to measure the sheet resistance, *R*s, at various angles, θ, relative to the flow direction at the same location. The sheet resistances, R_s, of three AgNW coatings with different degrees of alignment are plotted in Fig. 3A as a function of θ. For samples with good alignment, we find significant differences in measured sheet resistance at different angles. At the angle parallel to the flow direction, *i.e.* $\theta = 0°$ and 180°, the measured R_s values are in the range of 3–5 Ω sq^{-1}. However, at $\theta = 90°$ and 270°, R_s increases to ~42 Ω sq^{-1}, *i.e.*, an order of magnitude higher. Accordingly, we extract the angle-dependent sheet resistance of these aligned samples as follows:

$$R_{s,\theta} = a\sin(\theta) + R_0. \quad (3)$$

Here a and R_0 are fitting parameters. We find a good agreement between the data and the sinusoidal waveform. By con-

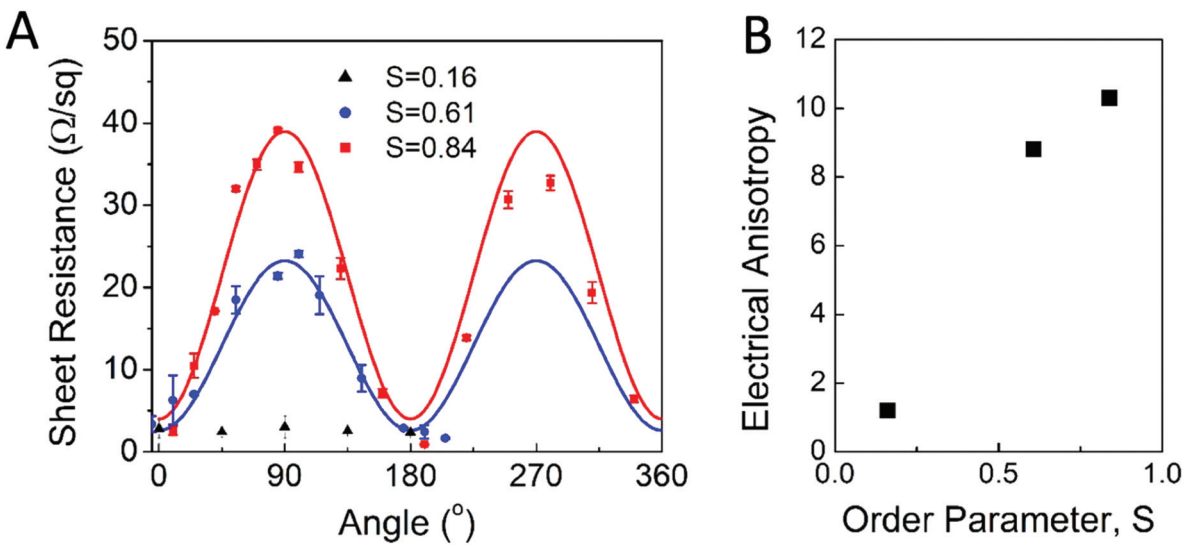

Fig. 3 Angle-dependent sheet resistance of the AgNW coatings. (A) Sheet resistance as a function of measurement angle relative to the alignment of the AgNW coatings (*i.e.*, with order parameters of 0.84, 0.61, and 0.16). Solid lines are fits to a sinusoidal function. (B) Electrical anisotropy as a function of order parameter.

trast, the sheet resistance for a AgNW coating with random orientations shows no angle dependence and measures ~3 Ω sq^{-1} for all angles.

To further quantify the effect of alignment, we define the electrical anisotropy, σ_{ani}, as the ratio between maximum and minimum sheet resistance measured at different angles, *i.e.* $\sigma_{ani} = R_{s,max}/R_{s,min}$, and we plot the ratio as a function of the AgNW coating order parameter, S (Fig. 3B). A strong anisotropy, σ_{ani}, up to ~10 is reached for highly aligned AgNW coatings (S = 0.84). We note that alignment-induced electrical anisotropy has also been reported in coatings of carbon nanotubes (CNTs).[40] Our observations about the change of anisotropy with the degree of alignment, S, are roughly consistent with the results measured for the CNT coatings, which is well-described by a model assuming a Gaussian distribution of the orientations of 1D conducting elements on a planar substrate. Anisotropy of electrical conductivity in aligned AgNW coatings has been reported. Ackermann *et al.*[42] reported σ_{ani} varying from 1.06 to 27.6. However, high electrical anisotropy, *i.e.* σ_{ani} > 2, was observed only in samples with a sheet resistance larger than 100 Ω sq^{-1}. To our knowledge, the well-aligned AgNWs used in the present work are the first to exhibit a large anisotropy (~10) while maintaining low sheet resistance (<50 Ω sq^{-1}) in all directions.

Optical anisotropy

Interestingly, the anisotropy of the coatings has a direct impact on their optical properties. We characterize the optical response of coatings made of aligned AgNWs using the setup shown in Fig. 4A. In this setup, the sample is illuminated with a Tungsten halogen light source (HL-2000, Ocean Optics) at normal incidence angle (along the $-z$ direction), and the AgNW coatings are placed in the xy-plane. The camera or detector is placed in the xz-plane with the polar angle, ϕ, measured relative to the z-axis. The angle between the polarization of the incident light and the y-axis is defined as α. For aligned AgNW coatings, the angle between the nanowire alignment direction and the y-axis is defined as β.

The images in Fig. 4B show the optical images of a well-aligned AgNW coating (S = 0.84) with light polarized along the y-axis (α = 0°) and x-axis (α = 90°), recorded at ϕ = 60°. The sample appearance varies from orange to yellow-green when α

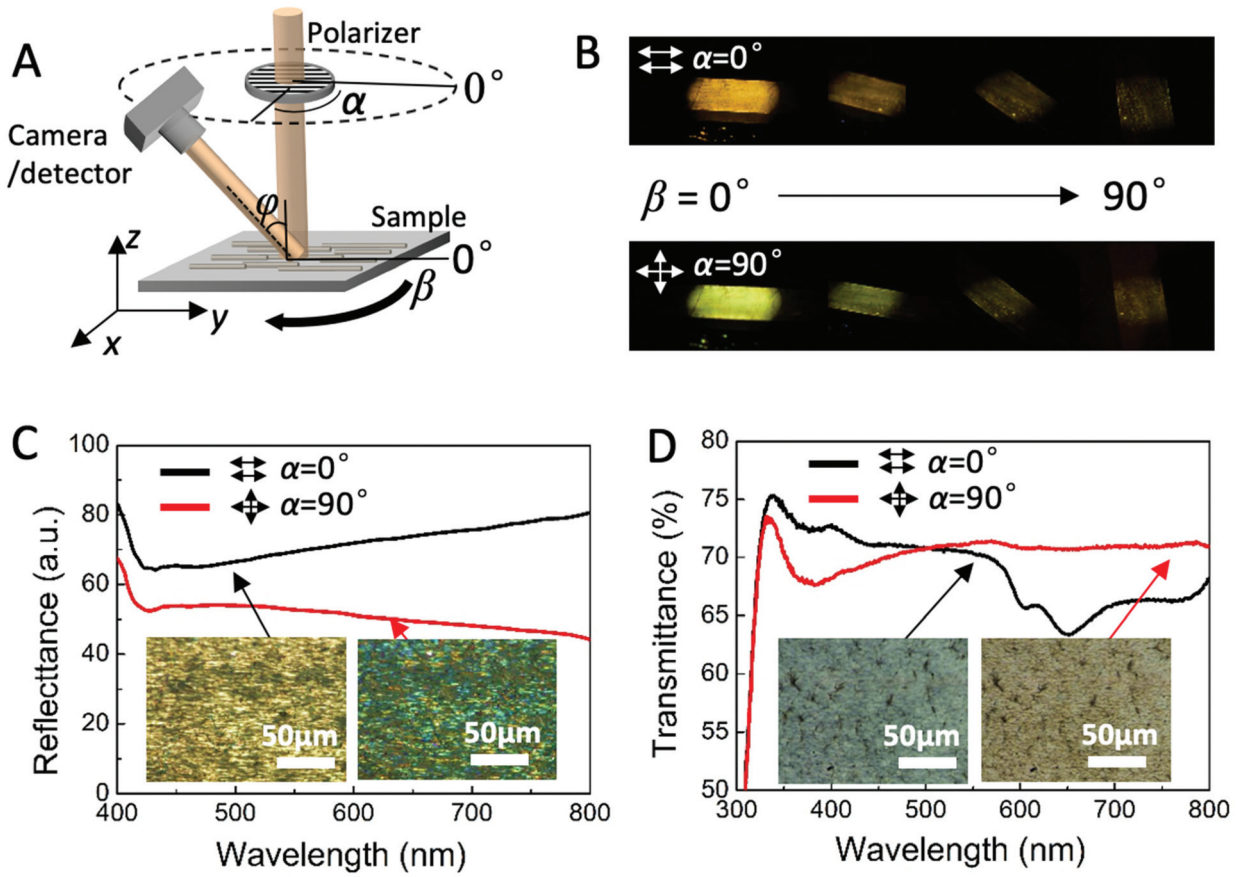

Fig. 4 Angle-dependent optical properties of the aligned AgNW coating (S = 0.84) under polarized illumination. (A) Schematic of the optical measurement setup showing the angles of AgNW alignment (β), polarization of incident light (α), and observation location (ϕ). (B) Photos taken at ϕ = 60° and various β angles when the incident light is polarized parallel (top) and perpendicular (bottom) to the AgNW alignment direction. (C) Spectrum of reflected light for two different input polarization configurations: parallel (black line) and perpendicular (red line) to the AgNW alignment direction. Insets: optical micrographs of the AgNW coating in reflection. (D) Spectrum of transmitted light under parallel and perpendicular illumination. Insets: optical micrographs of AgNW coatings in the transmission mode.

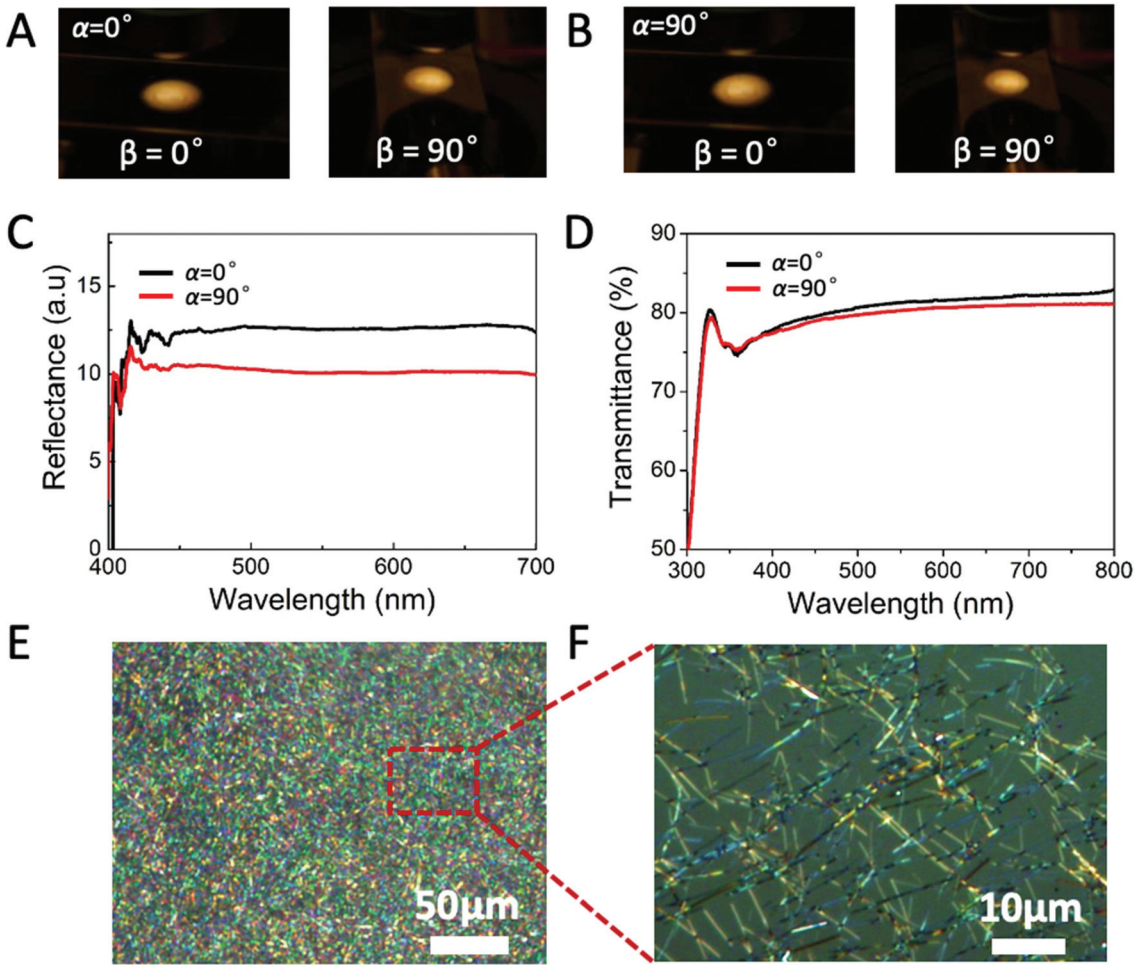

Fig. 5 Angle-independent optical appearance and spectrum of randomly oriented AgNW coatings under polarized light. (A) and (B) are photos of a random AgNW coating taken at various β angles, under incident polarization of α = 0° (A) or α = 0°. (B) Isotropic coatings appear the same under different polarization and observation angles; (C) and (D) spectra of reflected and transmitted light by randomly oriented AgNW coatings. (E) Micrograph of a randomly orientated AgNW coating under polarized light showing colors due to distributions of individual nanowires; (F) zoom-in view showing individual AgNWs that exhibit different colors depending on their orientations.

changes from 0° to 90°. In addition, a sharp decrease of the scattered light intensity occurs when β is rotated from 0° to 90°, for both α = 0° and α = 90°. By contrast, the color and intensity of the coatings of poorly aligned AgNWs remain the same (Fig. 5A and B).

We further investigate the color-changing mechanism by taking micrographs of the AgNW coatings using a microscope with a polarized light source. As shown in the insets in Fig. 4C, under the reflection mode, *i.e.* ϕ = 0°, and when the polarization and the AgNWs are aligned (α = 0° and β = 0°), the sample is mostly yellow. By contrast, the sample appears blue-green when the polarizer is perpendicular to the AgNW alignment (α = 90° and β = 0°). In the transmission mode (ϕ = 180°), the trends are opposite, as shown in the insets in Fig. 4D.

To more quantitatively explain the color differences, the reflectance and transmittance spectra are recorded. As shown in Fig. 4C, when α = 0°, the intensity of reflected light increases as a function of wavelength between 420 nm and 800 nm. When α = 90°, however, the reflected intensity decreases. These findings are consistent with the colors observed from the optical microscope (insets in Fig. 4C).

The transmittance spectra recorded using the UV-Vis spectrometer are plotted in Fig. 4D. While we did not optimize for transparency, the films retained good light transmission across the visible spectral range (~70%). The aligned AgNW coatings exhibit absorbing valleys for illumination in both polarization directions. However, these two valleys are centered at two very different wavelengths. For α = 0° and β = 0°, a strong absorption peak arises at long wavelengths, within the range of 600–650 nm, as shown in Fig. 4D. For α = 90° and β = 0°, the peak absorption arises at much shorter wavelengths, *i.e.*, ~380 nm. These spectra exhibit features similar to those of spectra reported for AgNWs in solution[43] and aligned AgNW bundles.[30,33] Prior simulation[44] and experimental[11,33,45] work explains the absorption peak at short (long) wavelength as due

to the transverse (longitudinal) surface plasmon resonance (SPR) of the electrons in the AgNWs.[30] Specifically, the absorption peak at short wavelength is due to the transverse surface plasmonic resonances (SPRs) induced by electron oscillation along the AgNW diameter, and the absorption at the long wavelength is due to the longitudinal SPRs (induced parallel to the AgNW long axis). The broadening of the peaks could be due, in part, to the polydispersity in the AgNW distribution and to the coupling of electromagnetic waves among neighboring nanowires.

When stimulated by polarized light, the wavelength of the absorption peak depends on the angle between the individual nanowire and the light polarization. This angle-dependent absorption is clearly seen in the micrographs of randomly oriented AgNWs in Fig. 5E and F, where an individual AgNW imaged in transmission appears yellow or green depending on its orientation relative to the light polarization. However, because of the random orientation of AgNWs, the overall spectra of the whole AgNW coating do not show absorption valleys, as seen in Fig. 5C and D. By contrast, when AgNWs are aligned along the same direction, the SPR absorption spectra of the aligned individual AgNWs are approximately the same and the sample as a whole exhibits a clear valley in its transmission spectra, as shown in Fig. 4D and E.

We systematically quantify the angle-dependent light intensity under various illumination and observation configurations to fully explore the optical anisotropy of the strongly aligned AgNW coating (S = 0.84) at 650 nm. The polar plot in Fig. 6A shows the intensity, I, of the reflected light, *i.e.* ϕ = 0°, as a function of the angle between the input polarizer and the AgNW alignment direction. The plot in Fig. 6A clearly demonstrates optical anisotropy; however, the value, $\frac{I_{max}}{I_{min}} = 1.7$, is rather small and the normalized light intensity peak at 180° is

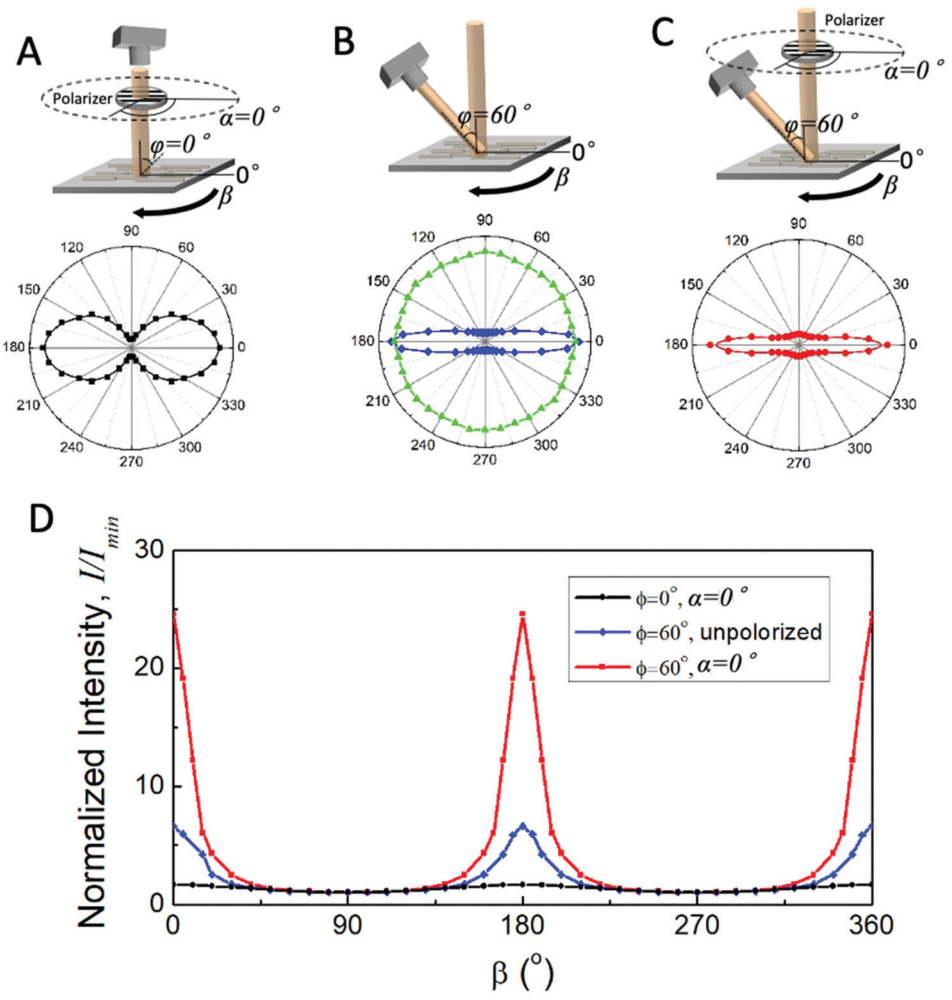

Fig. 6 Angle-dependent light intensity from aligned AgNW coatings. (A) Reflected light intensity (ϕ = 0°) as a function of β angles when the incident light (650 nm) is polarized parallel to the AgNW alignment direction (α = 0°); (B) scattered light intensity (ϕ = 60°) as a function of β when random (green) and well-aligned (blue, S = 0.84) AgNW coatings are illuminated with unpolarized light; (C) scattered light intensity (ϕ = 60°) as a function of β when the incident light is polarized parallel to the AgNW alignment direction (α = 0°); (D) normalized light intensity *vs.* β for a well-aligned AgNW (S = 0.84) coating under different illumination and observation configurations.

quite broad with a Full-Width-at-Half-Maximum (FWHM) of approximately 92°. This result is consistent with previous studies where weak optical anisotropy (<2×) is observed from individual aligned nanotubes and from AgNWs in both transmission and reflection modes.[10,11,46]

Next, we illuminate the aligned AgNW coating with unpolarized light and measure the intensity of scattered light at ϕ = 60°; for this measurement, the angle of the aligned AgNW coating, β, is varied by rotating the sample. The results are shown in Fig. 6B, which exhibits a large anisotropy, $\frac{I_{max}}{I_{min}} = 7.2$, and a narrow peak of normalized intensity with a FWHM of approximately 24°. For comparison, the intensity of unpolarized light scattered by a coating with randomly oriented AgNWs shows no variation as a function of β. These results indicate that the coating with aligned AgNWs scatters more light in the direction perpendicular to the AgNW alignment direction, and less light in the direction parallel to the alignment direction. This type of effect is observed in optical gratings with a parallel stripe structure on the surface.[47] It is also worth noting that the aligned AgNW coating scatters less light in total when integrating over β, compared to a randomly oriented AgNW coating. This scattering could potentially affect the haze of the coating. Reduction of haze by alignment has been studied previously[31] and is expected to decrease with better alignment, but we leave quantification of haze in our samples for future work.

Finally, we combine the two anisotropic effects by measuring the intensity of light scattered from the polarized light source. Specifically, for α = 0°, the intensity of scattered light at a constant azimuthal ϕ = 60° is measured as a function of different angles β. As shown in Fig. 6C, this configuration produces a very large optical anisotropy, with $\frac{I_{max}}{I_{min}} = 25.6$, and a very narrow peak, with a FWHM of approximately 15°. The comparison of normalized light intensity *versus* β for various values of α is shown in Fig. 6D. Clearly, the directional alignment of AgNWs, together with the polarization optical absorption and scattering properties of the individual AgNWs contribute to the overall optical anisotropy of the well-aligned AgNW coating. When the two mechanisms are combined, we observe a much higher anisotropy than reported in earlier studies.[10,11,46]

Large optical anisotropy has been shown to improve the resolution of signals such as those arising in polarization images or surface-enhanced Raman spectroscopy (SERS),[30] and large anisotropy is desirable in nanowire-based polarizers for polarization light sensors. Normally, researchers can use the different responses of aligned metal nanowires under different polarization light conditions to achieve optical anisotropy. Previous studies showed that transmission or reflection modes typically give an optical anisotropy of less than 2×,[11,25] in agreement with the results shown in Fig. 6A. Here, we have uncovered a novel way to further increase the optical anisotropy that relies on the light *scattered* by the aligned AgNWs. This detection configuration, wherein well-aligned AgNW coatings are illuminated with polarized light and the light scattered by the coating is detected at different polar angles, takes advantage of both the intrinsic polarization properties of AgNWs and the angle-dependent scattering of the aligned AgNWs to achieve greater optical anisotropy, which can be as large as 25× as demonstrated in Fig. 6C.

Conclusions

We developed a simple and robust flow-induced alignment method for preparing centimeter-scale planar conductive silver nanowire coatings with high degrees of anisotropy. Specifically, we demonstrated patterning of a 5 mm by 2 cm film strip of AgNWs with an orientation order parameter that was tunable from 0.16 to 0.84 and had concomitant variations in electrical and optical anisotropy. The alignment can be tuned by varying the shear rate of the nanowire suspension near the substrate during the deposition process. As a result of the preferred direction of AgNWs, coatings consisting of highly aligned AgNWs exhibit large anisotropy in both electrical conductivity and optical properties. For electrical conductivity, an anisotropy of ~10× is achieved, while the overall sheet resistance remains low. A very large optical anisotropy of ~25× is observed in the scattered polarized light due to the combination of the intrinsic polarization property of individual AgNWs and "grating" effects of the aligned AgNW network. Those highly conductive transparent coatings with large electrical and optical anisotropy can be potentially used for design of novel flexible antennas and polarized-light-based sensors and for surface enhanced Raman spectroscopy.

Experimental section

Silver nanowire suspension

The silver nanowires (AgNWs) were purchased from BlueNano (SLV-NW-90). The average length and diameter of the nanowires are 30 ± 5 μm and 90 ± 20 nm, respectively. The nanowires are suspended in ethanol at a solid concentration of 1 wt%. The nanowire suspension was used as received.

Assembly of the microfluidic channel

To fabricate the channels, two glass slides are attached (sandwiched) using two strips of double-sided tape, leaving a thin gap, as shown in Fig. 1A. The resulting rectangular channels are typically 25 mm in length, 5 mm in width, and 200 to 600 μm in height. The two open ends of the channel are then connected to a syringe filled with the AgNW suspension and a waste bottle.

Electrical characterization

The sheet resistances of the resulting AgNW coatings are measured using a four-point probe setup to eliminate the effect of contact resistance between the electrodes and coatings. Four electrical probes made of thin gold wires are arranged to be parallel and equally spaced. The part of the probe that comes into contact with the nanowire coating has a

length w = 2 mm, and each probe is separated by d = 0.5 mm, as shown in Fig. S3 in the ESI.† A constant DC current, I, is applied through the two outmost probes, and the voltage, U, is measured between the two inner probes. The sheet resistance, R_s, is then calculated by

$$R_s = \frac{U}{I}\frac{w}{d}, \quad (3)$$

where R_s has a unit of Ω sq^{-1}. This setup permits measurement of the intrinsic electrical conductivity of the nanowire coatings. To explore the angle-dependence of surface conductivity of our AgNW coatings, we place the coatings on a rotating stage wherein R_s can be measured at various angles relative to the flow direction at the same location.

Optical characterization

The micrographs of AgNW samples are recorded using an optical microscope (Olympus BX61) in both transmission and reflectance modes. In addition, the reflectance and transmittance spectra are recorded by coupling, respectively, a fiber spectrometer (USB4000, Ocean Optics) and a UV-Vis spectrometer (Cary 5000, Agilent Technologies) to an Olympus microscope.

Author contributions

Y.X., D.G., and A.G.Y. conceived and designed the project; Y.X., G.A.C., A.A., and D.K. carried out experiments for sample preparation; Y.X., A.L.E., and J.M.K. carried out electrical characterization experiments; D.G. and C.B. carried out optical characterization experiments; Y.X., D.G., R.D., and A.G.Y. analyzed the data and wrote the manuscript. All authors discussed the results and commented on the manuscript.

Conflicts of interest

There are no conflicts to declare.

Acknowledgements

We thank Prof. Karen Winey for helpful discussions. The project is supported by the National Science Foundation through DMR16-07378, MRSEC DMR-1720530, including both its Optical Microscopy and its Properties Measurement Shared Experimental Facilities, MRSEC DMR11-20901, and NASA 80NSSC19K0348. This work is also supported in part by Fundamental Research Funds for the Central Universities, the National Natural Science Foundation of China through Grant No. 11674019 (Y. X.) and 51973033 (D. G.), and Projects from Shanghai Science & Technology Commission 17JC1400700 and 17ZR1440000.

References

1 D. J. Finn, M. Lotya and J. N. Coleman, *ACS Appl. Mater. Interfaces*, 2015, **7**, 9254–9261.
2 J. Liang, K. Tong and Q. Pei, *Adv. Mater.*, 2016, **28**, 5986–5996.
3 E. M. Freer, O. Grachev, X. Duan, S. Martin and D. P. Stumbo, *Nat. Nanotechnol.*, 2010, **5**, 525–530.
4 F. Xu and Y. Zhu, *Adv. Mater.*, 2012, **24**, 5117–5122.
5 L. Hu, H. S. Kim, J. Y. Lee, P. Peumans and Y. Cui, *ACS Nano*, 2010, **4**, 2955–2963.
6 J. Yao, H. Yan, S. Das, J. F. Klemic, J. C. Ellenbogen and C. M. Lieber, *Proc. Natl. Acad. Sci. U. S. A.*, 2014, **111**, 2431–2435.
7 D. Rossouw, M. Couillard, J. Vickery, E. Kumacheva and G. A. Botton, *Nano Lett.*, 2011, **11**, 1499–1504.
8 L. Song, A. C. Myers, J. J. Adams and Y. Zhu, *ACS Appl. Mater. Interfaces*, 2014, **6**, 4248–4253.
9 L. Lu, L.-L. Wang, C.-L. Zou, X.-F. Ren, C.-H. Dong, F.-W. Sun, S.-H. Yu and G.-C. Guo, *J. Phys. Chem. C*, 2012, **116**, 23779–23784.
10 X. Ma, X. Zhu, F. You, J. Feng, M.-C. Wang and X. Zhao, *J. Alloys Compd.*, 2014, **592**, 57–62.
11 J. W. Liu, J. L. Wang, W. R. Huang, L. Yu, X. F. Ren, W. C. Wen and S. H. Yu, *Sci. Rep.*, 2012, **2**, 987.
12 R. M. Mutiso and K. I. Winey, *Phys. Rev. E: Stat., Nonlinear, Soft Matter Phys.*, 2013, **88**, 032134.
13 R. M. Mutiso, M. C. Sherrott, A. R. Rathmell, B. J. Wiley and K. I. Winey, *ACS Nano*, 2013, **7**, 7654–7663.
14 S. White, B. DiDonna, M. Mu, T. C. Lubensky and K. I. Winey, *Phys. Rev. B: Condens. Matter Mater. Phys.*, 2009, **79**, 024301.
15 D. Zhang, Y. Xiang, J. Chen, J. Cheng, L. Zhu, R. Wang, G. Zou, P. Wang, H. Ming, M. Rosenfeld, R. Badugu and J. R. Lakowicz, *Nano Lett.*, 2018, **18**, 1152–1158.
16 A. W. Sanders, D. A. Routenberg, B. J. Wiley, Y. Xia, E. R. Dufresne and M. A. Reed, *Nano Lett.*, 2006, **6**, 1822–1826.
17 W. Wang, Q. Yang, F. Fan, H. Xu and Z. L. Wang, *Nano Lett.*, 2011, **11**, 1603–1608.
18 X. Guo, M. Qiu, J. Bao, B. J. Wiley, Q. Yang, X. Zhang, Y. Ma, H. Yu and L. Tong, *Nano Lett.*, 2009, **9**, 4515–4519.
19 D. Lei, A. Aubry, Y. Luo, S. A. Maier and J. B. Pendry, *ACS Nano*, 2011, **5**, 597–607.
20 S.-k. Duan, Q.-l. Niu, J.-f. Wei, J.-b. He, Y.-a. Yin and Y. Zhang, *Phys. Chem. Chem. Phys.*, 2015, **17**, 8106–8112.
21 Y. J. Jeon, H. W. Kang, S. H. Ko and H. J. Sung, *Meas. Sci. Technol.*, 2013, **24**, 035303.
22 Y. Li and Y. Wu, *J. Am. Chem. Soc.*, 2009, **131**, 5851–5857.
23 Y. Liu, J. H. Chung, W. K. Liu and R. S. Ruoff, *J. Phys. Chem. B*, 2006, **110**, 14098–14106.
24 S. J. Papadakis, Z. Gu and D. H. Gracias, *Appl. Phys. Lett.*, 2006, **88**, 233118.
25 H.-Y. Shi, B. Hu, X.-C. Yu, R.-L. Zhao, X.-F. Ren, S.-L. Liu, J.-W. Liu, M. Feng, A.-W. Xu and S.-H. Yu, *Adv. Funct. Mater.*, 2010, **20**, 958–964.

26 W. Yang, L. Qu, R. Zheng, Z. Liu, K. R. Ratinac, L. Shen, D. Yu, L. Yang, C. J. Barrow, S. P. Ringer, L. Dai and F. Braet, *Chem. Mater.*, 2011, **23**, 2760–2765.
27 R. Zhu, Y. Lai, V. Nguyen and R. Yang, *Nanoscale*, 2014, **6**, 11976–11980.
28 L. Meng, R. Bian, C. Guo, B. Xu, H. Liu and L. Jiang, *Adv. Mater.*, 2018, **30**, 1706938.
29 C. D. Preston, L. Hu and L. J. Martínez-Miranda, *Mol. Cryst. Liq. Cryst.*, 2015, **610**, 235–239.
30 A. Tao, F. Kim, C. Hess, J. Goldberger, R. He, Y. Sun, Y. Xia and P. Yang, *Nano Lett.*, 2003, **3**, 1229–1233.
31 S. Kang, T. Kim, S. Cho, Y. Lee, A. Choe, B. Walker, S. J. Ko, J. Y. Kim and H. Ko, *Nano Lett.*, 2015, **15**, 7933–7942.
32 Y. Ko, S. K. Song, N. H. Kim and S. T. Chang, *Langmuir*, 2016, **32**, 366–373.
33 B. Park, I. G. Bae and Y. H. Huh, *Sci. Rep.*, 2016, **6**, 19485.
34 S. Cho, S. Kang, A. Pandya, R. Shanker, Z. Khan, Y. Lee, J. Park, S. L. Craig and H. Ko, *ACS Nano*, 2017, **11**, 4346–4357.
35 Y. Huang, X. Duan, Q. Wei and C. M. Lieber, *Science*, 2001, **291**, 630–633.
36 F. L. Leite, C. C. Bueno, A. L. Da Roz, E. C. Ziemath and O. N. Oliveira, *Int. J. Mol. Sci.*, 2012, **13**, 12773–12856.
37 S. B. Kharchenko, J. F. Douglas, J. Obrzut, E. A. Grulke and K. B. Migler, *Nat. Mater.*, 2004, **3**, 564–568.
38 M. Liu, Y. Chen, Q. Guo, R. Li, X. Sun and J. Yang, *Nanotechnology*, 2011, **22**, 125302.
39 P. J. Steinhardt, D. R. Nelson and M. Ronchetti, *Phys. Rev. B: Condens. Matter Mater. Phys.*, 1983, **28**, 784–805.
40 C. Zamora-Ledezma, C. Blanc, N. Puech, M. Maugey, C. Zakri, E. Anglaret and P. Poulin, *Phys. Rev. E: Stat., Nonlinear, Soft Matter Phys.*, 2011, **84**, 62701.
41 M. Doi and S. F. Edwards, *The theory of polymer dynamics*, Oxford University Press, 1988.
42 T. Ackermann, R. Neuhaus and S. Roth, *Sci. Rep.*, 2016, **6**, 34289.
43 Q. N. Luu, J. M. Doorn, M. T. Berry, C. Jiang, C. Lin and S. P. May, *J. Colloid Interface Sci.*, 2011, **356**, 151–158.
44 J. Dong and I. A. Goldthorpe, *Nanotechnology*, 2017, **29**, 45705.
45 B. Pietrobon, M. McEachran and V. Kitaev, *ACS Nano*, 2009, **3**, 21–26.
46 M. F. Islam, D. E. Milkie, C. L. Kane, A. G. Yodh and J. M. Kikkawa, *Phys. Rev. Lett.*, 2004, **93**, 37404.
47 G. J. Dunning and M. L. Minden, *Appl. Opt.*, 1980, **19**, 2419.

